RSC Advances

REVIEW

View Article Online
View Journal | View Issue

Cite this: *RSC Adv.*, 2014, **4**, 58090

Nanomaterials *via* solution combustion synthesis: a step nearer to controllability

Wei Wen[a] and Jin-Ming Wu*[b]

Solution combustion synthesis (SCS) is a worldwide adopted technique to synthesize nanomaterials, especially for oxides, because of its simplicity, energy and time-effectiveness, and low cost. The general difficulty encountered in SCS is the controllability over phases and morphologies of the products, which arises from the inherent rapid and uncontrollable combustion procedure. In this regard, the present work is devoted to review the recent progress on phase- and morphology-controlled SCS in detail. Besides the various metal oxides, SCS is now applicable to fabricate nanomaterials of metal phosphates, metal silicates, metal borates, metal sulfides, metals, and even alloys, through careful selection of solution compositions. Oxides with regular morphologies of flowers, belts, triangles, tubes, wires, and rods can be synthesized by SCS, in the presence of certain templates, or through a self-assembly procedure. The recent progress made on the synthesis of porous materials *via* SCS is summarized. SCS is also capable of growing metal oxide thin films at low temperatures, enabling the fabrication of low-cost and high-performance electronics on flexible plastic substrates.

Received 10th September 2014
Accepted 30th October 2014

DOI: 10.1039/c4ra10145f

www.rsc.org/advances

1. Introduction

Nanomaterials have sparked worldwide interest because of their unique physical and chemical properties arising from their small dimensions when compared with those of their bulk counterparts. In industry, oxide powders are generally fabricated by high-temperature solid-state reactions, where the desired products are achieved simply by maintaining the solid mixture of reactants at a high temperature.[1,2] Such a ceramic route is energy and time consuming, and the products are usually inhomogeneous, coarse, impure, and away from stoichiometry because of a big diffusion barrier resulted from the lack of molecular-level mixing. Combustion synthesis (CS) is just the choice to achieve a rapid and energy-efficient synthesis. A typical CS procedure utilizes a self-sustained exothermic reaction among well-mixed reactants to achieve the rapid and economical synthesis of particulate products. Up to 2008, CS has been adopted to fabricate more than 1000 kinds of oxide powders[3] over more than 65 countries.[4]

[a]*College of Mechanical and Electrical Engineering, Hainan University, Haikou 570228, P. R. China*

[b]*State Key Laboratory of Silicon Materials, Key Laboratory of Advanced Materials and Applications for Batteries of Zhejiang Province, Department of Materials Science and Engineering, Zhejiang University, Hangzhou 310027, P. R. China. E-mail: msewjm@zju.edu.cn*

Wei Wen obtained his Ph.D. degree in Materials Science and Engineering from Zhejiang University in 2014. Currently, he is an assistant professor at the College of Mechanical and Electrical Engineering, Hainan University. His work is devoted to wet-chemistry synthesis of nanostructured oxides and their functional applications.

Jin-Ming Wu is a professor at the State Key Laboratory of Silicon Materials, Zhejiang University. In 1999, he obtained his Ph. D. degree in Materials Science from Zhejiang University. He worked as a VBL researcher in Okayama University, Japan during the year 2000-2002 and an Alexander von Humboldt research fellow in Max-Planck-Institute of Colloids and Interfaces, Germany, from 2006 to 2007. His work is devoted to nanostructured oxides for energy and environmental applications.

Based on the physical nature of the reactants and also reaction mediums, CS can be classified as self-propagating high temperature synthesis (SHS) and solution combustion synthesis (SCS).[4–6] Various materials of oxides, carbides, nitrides, borides, and aluminides have been obtained by SHS, some of which have been commercialized successfully.[7–9] In industry, ceramic-lined steel pipes have also been prepared by a centrifugal SHS.[10] The reactants in conventional SHS are all in solid state, still suffering from an inhomogeneous mixing. The coarse initial powders (10–100 μm in size) and high reaction temperatures (>2000 K) result in products with low surface areas and coarse sizes.[4,5] Additional treatments such as mechanical activation,[11] intensive milling,[12] or chemical dispersion[4,13] are required after SHS to reduce the particle size, which increase the preparation steps and cost. On the contrary, SCS begins from an aqueous solution, which guarantees a molecular-level mixing of reactants. As a result, SCS serves as a promising route for rapid and direct synthesis of mass nanomaterials.

2. Solution combustion synthesis (SCS)

In 1988, Patil firstly reported the synthesis of Al_2O_3 using $Al(NO_3)_3 \cdot 9H_2O$ and urea.[14] A typical SCS relies on an exothermic reaction between an oxidizer, typically metal nitrates, like $Al(NO_3)_3 \cdot 9H_2O$, and an organic fuel such as urea. The driving force for lattice formations derives from the internal chemical energy. The temperature input for SCS is not high, which is required just to trigger the combustion reaction, rather than to provide a continuous energy input to form lattices as the case in conventional material fabrication routes. Various water-soluble organics containing large quantities of C and H are utilized as fuels, which facilitates the liberation of heat by combustion. Certain fuels, such as glycine, also form complexes with metal ions to improve the mixing level of the reactants.[5,15] For example, citric acid bonds with metal ions to form stable chelate complex compounds; amino acids, such as glycine, bonds with metal ions to build very stable chelate complex compounds. The formation of complex helps to achieve a more homogeneous mixing and hence avoids segregations, which is beneficial for producing complex and multicomponent oxides.[16]

Most of the solution combustion procedures involve a transition from solution to a colloidal sol and then to a gel, which are thus also termed as gel (or sol–gel) combustion. Based on the precursors utilized, the sol–gel method can be categorized into three types: hydrolysis-condensation of metal-alkoxides, the gelation route *via* concentration of aqueous solutions involving metal-chelates, and the Pechini method.[17] Among them, the Pechini technique includes a combined process of metal complex formation and *in situ* polymerization of organics and is versatile for fabricating metal oxides with homogeneous multicomponents.[17] A typical Pechini procedure involves the introduction of metal salts or alkoxides into an ethylene glycol solution that contains citric acid. The formation of citric complexes leads to a homogeneous mixing and avoids the separation of components at the later stage. The polycondensation of citric acid and ethylene glycol results in the polymer gel formation. A subsequent heating of the gel leads to the removal of the polymer matrix and the formation of the products with a good homogeneity. If metal nitrates are used, instead of the metal salts or alkoxides, as precursors, and fuels are used as complexing agents, the Pechini sol–gel routes would involve a combustion reaction during the final heating process.

In SCS, the phase, morphology, particle size and surface area of products can be altered to certain extents by adjusting the fuel, the fuel/oxidizer ratio, and the pH value of the solution.[15,16] A higher combustion temperature during SCS usually results in improved crystallinity, larger grain size, more serious agglomeration, and lower specific surface area for the products. The propellant chemistry theory is usually used to calculate the stoichiometry of the fuel and oxidizer.[18,19] Taking the combustion reaction between zinc nitrate and urea (CH_4N_2O) as an example, the elemental valency of Zn, C, H, N, and O is +2, +4, +1, 0, and −2, respectively. Accordingly, the oxidizing valency of zinc nitrate and the reducing valency of urea are −10 and +6, respectively. The equilibrium combustion reaction can be described as,

$$Zn(NO_3)_2 + \frac{5}{3}\varphi CH_4N_2O + 5(\varphi - 1)O_2 \rightarrow ZnO + \frac{5\varphi + 3}{3}N_2(g) + \frac{5}{3}\varphi CO_2(g) + \frac{10}{3}\varphi H_2O(g)$$

where, $\varphi = 1$ means a stoichiometric state, in which atmospheric oxygen is not needed for a complete oxidation of the fuel. $\varphi > 1$ and $\varphi < 1$ indicates a fuel-rich and fuel-lean condition, respectively. The fuel initiates the combustion reaction with metal nitrates at low ignition temperatures.[5] When $\varphi = 1$, the combustion is intense and complete, which releases lots of heat. $\varphi > 1$ or $\varphi < 1$ means one of the reactants is excess in the combustion system. Trace impurities, such as carbon and carbonates, would remain in the product, especially under a fuel-rich condition. The phase of products is also determined by the fuel/oxidizer ratio, because the fuel and metal nitrate acts as reducer and oxidizer, respectively. For example, an appropriate fuel/oxidizer ratio in a fuel-rich condition results in the formation of metal rather than metal oxides, as will be discussed latter in Section 3.2. A very high fuel/oxidizer ratio in a fuel-rich condition would result in the formation of amorphous metal complexes, which decompose to form porous metal oxides during the subsequent calcinations (as discussed latter in Section 4.2). Fig. 1 shows a typical combustion procedure for the synthesis of ZnO using urea as a fuel. The combustion reaction sustains after stopping the supply of external energy input, which demonstrates clearly a self-propagating nature of SCS.[20]

The advantages of SCS can be summarized as follows:[15,16,21] (1) time and energy efficient; (2) the equipment is simple and the raw materials are usually less expensive; (3) a molecular level mixing for the raw materials; and (4) the composition of products can be tuned. Thanks to such merits, SCS has been adopted to fabricate various materials for many applications of catalysis,[22–30] luminescent materials,[31–36] fuel cells,[37–39] energy conversion,[40–42] and energy storage.[43–46] Complicated Garnets

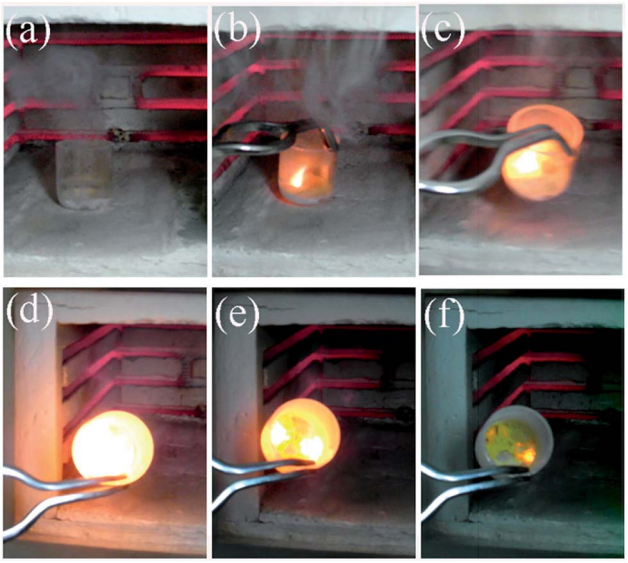

Fig. 1 The typical combustion procedure in SCS: (a) after complete dehydration but before combustion, (b) ignition, (c–f) the combustion process after stopping energy input by taking the reactor out of the oven.[20] Adopted from ref. 20, Copyright 2013, with permission from Elsevier.

are also widely synthesized by SCS.[47–50] For example, Huczko *et al.* synthesized cerium-doped yttrium aluminum garnet by SCS.[47] Recently, SCS is also applied to synthesize thin films of metal oxides.[51–55] Fabrications of low-cost and high-performance electronics at low temperatures are thus possible with the help of SCS.[51–55] A detailed description of SCS and its applications is out of the region of this review and the interested readers can refer to other reviews[3–6,21,22] and books.[15,16] For example, a book edited by Lackner *et al.*[16] described in detail the characteristics and mechanisms of SCS. The present review focus on the recent progress on SCS to fabricate nanomaterials with more controllable phase and morphology.

3. Phase control in SCS

Most of binary, ternary or even more complicated oxides have been achieved by SCS; on the contrary, reports on nanomaterials other than oxides are relatively rare. Encouragingly, it is reported that many phosphates can be obtained by SCS followed by a subsequent heat treatment, in the presence of additional $(NH_4)_2HPO_4$ or $NH_4H_2PO_4$.[56–61] Li_2SrSiO_4 (ref. 62) and Li_2FeSiO_4/C[63] are also prepared by SCS and a subsequent heat treatment, in which SiO_2 serves as a silica source. Wang *et al.* synthesized copper-doped $Li_2B_4O_7$ by SCS and a subsequent heat treatment, using H_3BO_3 as a boron source.[64] Recently, metal sulfides, pure metals, and alloys have been achieved by SCS *via* carefully selecting fuels, changing the ratio of fuel to oxidizer, and controlling the reaction atmosphere.

3.1 Synthesis of metal sulfides

Tukhtaev *et al.* used thiourea or thiosemicarbazide as a fuel, which also complexed with metal ions, to prepare various metal sulfides by SCS in an inert atmosphere.[65] The particle size and morphology of the products are reported to be dependent on the atmosphere pressure.[65] CdS with crystallite size of 10–15 nm was also obtained by a microwave-assisted combustion synthesis using thiourea as a fuel.[66] Amutha *et al.* also obtained CdS nanoparticles by the microwave-assisted combustion synthesis using cadmium thiocyanate complex as a single source precursor.[67] The key to achieve metal sulfides instead of the corresponding metal oxides is the selection of appropriate fuel, such as thiourea, which contains abundant sulfur. However, the fabrication of other metal sulfides beside CdS by SCS in an air atmosphere is rarely reported. Further work is needed to clarify the exact formation mechanism of CdS during SCS in an air atmosphere.

3.2 Synthesis of metals and alloys

Fuels in SCS act as reducing agents; therefore, it is possible to further reduce the metal oxides produced in SCS by the residual fuel. Rao *et al.* obtained metallic Cu, Ni, and CuNi alloys by SCS using *N*-tertiarybutoxy-carbonylpiperazine ($C_9H_{18}N_2O_2$) as a fuel.[68] Later, Jung *et al.* directly synthesized nickel particles through a microwave-induced SCS with a fuel-rich composition in an air atmosphere without a further reducing calcination process.[69] Erri *et al.* chose an appropriate fuel/oxidizer ratio to control the combustion velocity and thus a nickel foam was obtained.[70] The fuel-rich condition was demanded to provide a reducing atmosphere for the metallic Ni formation.[70]

Jiang *et al.* also used SCS to prepare various metal and alloy nanoparticles of Ni, Co, Cu, Ag, Bi, $Ni_{0.5}Co_{0.5}$ in an inert atmosphere.[71] H_2, H_2O, CH_4, NO, CO_2, NH_3, and NO_2 species were detected near the combustion temperature. Among them, H_2 and CH_4 have the reducing ability to obtain metals from the corresponding metal oxides. An appropriate fuel/oxidizer ratio is critical for the synthesis of metals by SCS. A low fuel/oxidizer ratio restricts the reduction reaction; however, when the ratio is too high, the combustion temperature decreases, which also inhibits the reduction of metal oxides.[71]

Mukasyan's group investigated the reaction pathways of metal nanopowders in SCS both in experiment and thermodynamic analysis, taking nickel[72] and copper[73] as a model, respectively. The formation of nickel oxide appeared at the early stage in the reaction front, followed by a reduction to nickel in the post combustion zone. The reducing environment was achieved in fuel-rich conditions.[72] Similar reaction pathways were also observed in a copper nitrate–glycine system.[73] Recently, they further used several *in situ* techniques and electron microscopy to study the mechanism in combustion reaction of a nickel nitrate–glycine system.[74] The results further confirmed that metal oxides formed at the early stage by decomposition of metal nitrate, which were then reduced to the corresponding metals by the reducing gases released in the combustion process in fuel-rich conditions.[74] In the nickel nitrate–glycine system, the source of energy for self-sustained reaction was the exothermic reaction between N_2O and NH_3 species from the decomposition of nickel nitrate and glycine.[74] The excess NH_3 gas produced in fuel-rich conditions reduces

nickel oxide to nickel in the reaction front.[74] The mechanism of combustion synthesis of Ni in nickel nitrate–glycine system is summarized in Fig. 2. It is not favorable to obtain metallic iron in the iron nitrate–glycine system because iron(II) oxide can not be reduced to iron by NH_3 (or H_2) even at 1500 °C, as suggested by a thermodynamic calculation.[74] Pure iron was recently prepared by combustion of an iron nitrate–citric acid system in a nitrogen atmosphere, using the mixture of ethanol and deionized water as a solvent.[75] Interestingly, Fe_3C was also obtained by further increasing the amount of citric acid (fuel).[75] It is also found that more completed reduction of $Ni_{1-x}Co_x$ alloys can be achieved by adding appropriate amounts of ethanol, which thus improves the saturation magnetization.[76] The additive of a suitable amount of ethanol was supposed to increase the reduction ability of the sol–gel combustion process.[75,76] The metals and alloys obtained by SCS, including Fe, Co, Ni, Cu, Ag, Bi, Ni–Co alloys, Ni–Cu alloys, and Ni–Cu–Fe alloys, are summarized in Table 1.

4. Morphology control in SCS

Controlling nuclei formation and the subsequent crystal growth is crucial for the synthesis of high-quality crystals with certain morphologies. The rapid combustion reaction and less controllable combustion process make it difficult to control the morphology of products in SCS. The typical morphology of products by SCS is agglomerations of irregular nanoparticles.

4.1 Products with regular shapes

Introducing appropriate templates in SCS results in special nanostructures. For example, hydroxylapatite nanotubes have been obtained by introducing a porous anodic aluminum oxide (AAO) template in SCS.[79] After the removal of the AAO template, uniform hydroxylapatite nanotubes with a fiber-brush like shape were obtained, as shown in Fig. 3a–c. The length and diameter of the nanotubes is *ca.* 60 μm and 100 nm, respectively. The TEM image (Fig. 3c) clearly shows the hollow structure. Just like other template-assisted synthesis methods, the

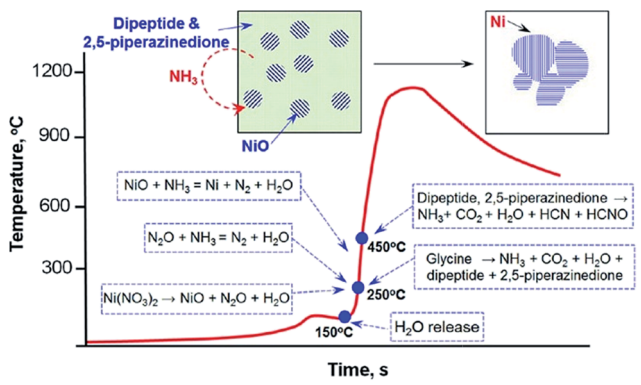

Fig. 2 A schematic illustration showing the mechanism of Ni formation during self-sustained combustion reactions of nickel nitrate–glycine gels.[74] Adopted from ref. 74, Copyright 2013, with permission from American Chemical Society.

Table 1 Various metals and alloys derived from SCS

Metals or alloys	Fuel	Other starting reactants	Fuel to oxidizer molar ratio	Atmosphere	Solvent	pH	Heating temperature/°C	Pre-dried temperature/°C	Ref.
Ni, Cu, and Ni–Cu	*N*-Tertiarybutoxy -carbonylpiperazine	Hydrated metal nitrates	1.0	Air	Water	\[a]	350	\[a]	68
Ni	Glycine	$Ni(NO_3)_2 \cdot 6H_2O$	2.44	Air	Water	\[a]	Microwave	\[a]	69
Ni, Cu, Co, Ni–Cu, and Ni–Co	Glycine	Hydrated metal nitrates	1.4 for Ni, 2.8 for Cu, and 1.7 for $Ni_{0.9}Cu_{0.1}$	Air	Water	\[a]	—[b]	\[a]	70
Co, Ni, Cu, Ag, Bi, and Ni–Co	Citric acid	Hydrated metal nitrates	0.8–1.2 for Ni	N_2	Water	7	300	95	71
Ni	Glycine	$Ni(NO_3)_2 \cdot 6H_2O$	1.4	Air	Water	\[a]	—[b]	—[b]	72
Cu and Ni–Cu	Glycine	Hydrated metal nitrates	3.3 for Cu and 1.9 for Cu–Ni	Air	Water	\[a]	—[b]	—[b]	73
Fe	Citric acid	$Fe(NO_3)_3 \cdot 9H_2O$	1.25	N_2	Water + ethanol	6	300, 400, 500, 600, 700	95	75
Ni–Co	Citric acid	Hydrated metal nitrates	1.0	N_2	Water + ethanol	7	300, 400, 500, 600, 700	90	76
Cu, Ag, and Ni	Glycine	Hydrated metal nitrates	2.0 for Ni	Air	Water	\[a]	250	\[a]	77
Ni–Cu–Fe	Glycine	Metal nitrates	1.9	Air	Water	\[a]	—[b]	—[b]	78

[a] \ means without treatment. [b] — means that it was not described in the reference.

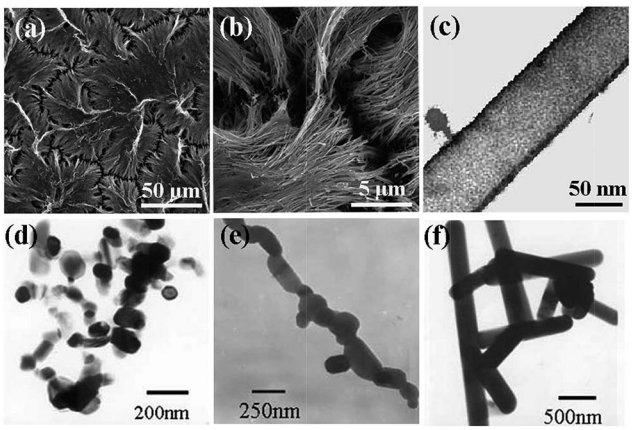

Fig. 3 SEM (a, b) and TEM (c) images of hydroxyapatite nanotubes.[79] TEM images of $CaIn_2O_4$: (d) as-combusted, (e) post-annealed at 1373 K for 2 h and (f) post-annealed at 1373 K for 12 h.[80] (a–c) adopted from ref. 79, Copyright 2008, with permission from Elsevier. (d–f) adopted from ref. 80, Copyright 2009, with permission from Springer.

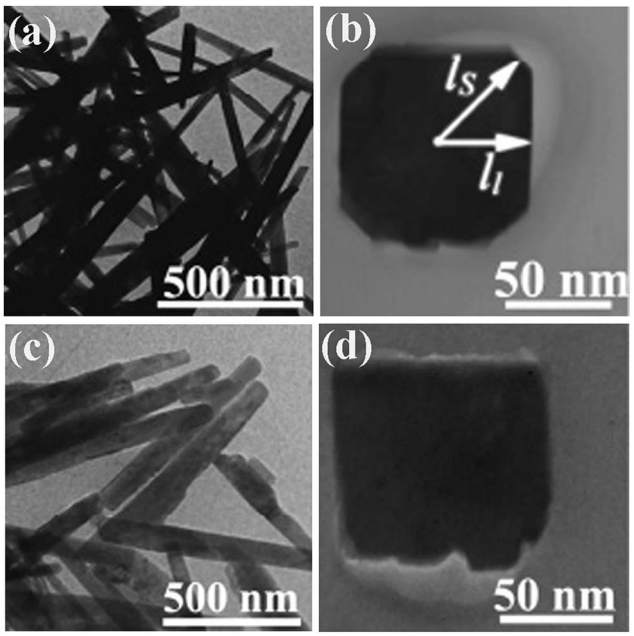

Fig. 4 TEM images of (a and b) $Al_4B_2O_9$ nanowires synthesized at 900 °C for 2 h and (c and d) $Al_{18}B_4O_{33}$ nanowires synthesized at 1050 °C for 2 h.[84] Adopted from ref. 84, Copyright 2007, with permission from American Chemical Society.

preparation and removal of templates make the synthesis procedure complex and expensive.

Interestingly, one-dimensional nanostructures can sometimes be obtained by annealing the preformed nanoparticles derived form SCS.[80–82] For example, Ding *et al.* obtained $CaIn_2O_4$ nanorods (Fig. 3f) by SCS combined with a high-temperature post-annealing.[80] Firstly, $CaIn_2O_4$ nanoparticles were formed by SCS (Fig. 3d). Then, the as-combusted $CaIn_2O_4$ nanoparticles self-assembled into nanocapsules and subsequently formed the regular rods (Fig. 3e and f). The formation of rods was believed to be related to the asymmetric crystal structure of $CaIn_2O_4$ and the instantaneous high temperature involved in the combustion.[80] V_2O_5 rods were also synthesized by SCS combined with a subsequent annealing at 550 °C for 24 h.[81] Chen *et al.* also obtained $Sn_{1-x}RE_xO_{2-x/2}$ (RE = Y, La, Gd and Nd) nanorods by annealing the as-synthesized products from a microwave-induced KCl-assisted SCS.[82] The diameter and length of the nanorods is 8–12 nm and 100–200 nm, respectively. The preformed nanoparticles by the KCl-assisted SCS transfer to nanorods in the molten salt during annealing.[82]

More interestingly, calcium phosphate nanowhiskers were directly prepared by a microwave-assisted auto ignition molten salt synthesis without the subsequent annealing.[83] $NaNO_3$ was used as fluxing agent and urea served as the fuel for combustion. The combustion process raises the extent of superheating in the molten-salt bath. Embryonic particles of calcium phosphates are formed through the nucleation and growth procedure. Calcium phosphate nanowhisker growth occurs by a sequential "dissolution–crystallization–whisker growth" process as the molten ionic bath cools down.[83] Tao *et al.* achieved single-crystalline $Al_4B_2O_9$ (Fig. 4a and b) and $Al_{18}B_4O_{33}$ nanowires (Fig. 4c and d) by the one-step high-temperature calcination at 900 °C and 1050 °C, respectively, in which the combustion were maintained for *ca.* 6 min and final products were obtain after 2 h annealing.[84] The cross-sectional observation reveals that the $Al_4B_2O_9$ nanowires, which grew along the [100] direction, exhibited four large facets with lower surface energy and four small facets with high surface energy (Fig. 4b). For the $Al_{18}B_4O_{33}$ nanowires, which grew along the [001] direction, the small facets with high surface area disappeared, resulting in a nearly square cross section (Fig. 4d). The anisotropical growth of both nanowires was believed to result from the requirement to minimize the surface energy for a free particle. The single crystalline nature for the nanowires with high purity seems to be the key to achieve the nanowires during the SCS procedure.

Cheng *et al.* used SCS followed by a subsequent high-temperature calcination to synthesize Eu^{3+} incorporated ZnO belts[85] (Fig. 5a and b) and $SrAl_xO_y : Eu^{2+}$, Dy^{3+} belts (Fig.5c and d).[86] The introduction of $N(CH_2CH_2OH)_3$ (triethanolamine, TEA) is believed to be the key to achieve the final specific morphology, because it is a multifunctional reagent serving simultaneously as a chelating agent to form metal–TEA complexes, a surfactant to control the shape of precursors, and also a fuel that is capable of reducing the reaction rate of the combustion synthesis.[85,86] Mapa *et al.* synthesized N doped ZnO micrometer-sized triangular particles (Fig. 5e) by a combustion reaction between urea and zinc nitrate with a molar ratio of *ca.* 1.[87] The size is relatively less uniform and is large in micro-scale rather than in nano-scale. The authors argued that, when the urea/$Zn(NO_3)_2$ molar ratio increased to beyond 3, an increasing exothermicity was achieved for the combustion reaction. As a result, no specific morphology can be observed for the resultant particles.[87] The triangular particles are believed to result from the stress-free and well-grown crystals, which is expected from slow crystallization. The exact mechanism for the formation of

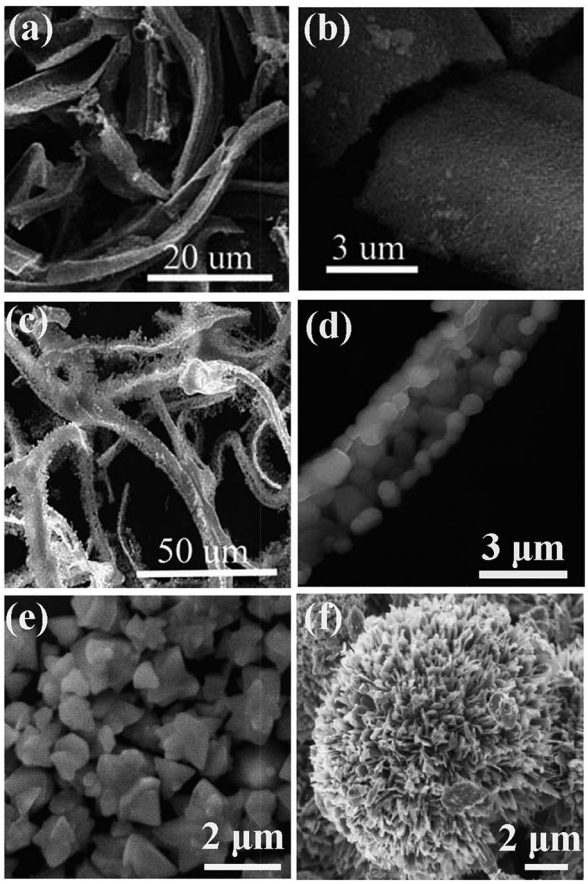

Fig. 5 SEM images of the ZnO post-annealing at 600 °C (a and b),[85] $SrAl_xO_y$ post-annealing at 1300 °C (c and d),[86] triangular ZnO (e),[87] and CuO nanoflowers (f).[88] (e) Adopted from ref. 87, Copyright 2009, with permission from American Chemical Society. (f) Adopted from ref. 88, Copyright 2013, with permission from Elsevier.

the triangular-shaped particles by SCS, which is indeed a rapid preparation method, is therefore surprising; however, Mapa's study suggests that, for polycrystalline oxides, a moderate combustion favors the formation of particles with specific morphologies.

Recently, copper oxide (CuO) nanoflowers, as shown in Fig. 5f, were prepared by SCS, where glycine was used as a fuel.[88] The CuO nanoflowers contain well-crystallized nanopetals/sheets. The flower-like structure was believed to come into being through the local sintering of the preformed nanoparticles during the high temperature combustion.

Although some progresses have been made, most of regular morphologies reported to date are in micro-scale or need a subsequent annealing. For the AAO-assisted SCS to obtain one-dimensional (1D) nanostructures, the penetration of the precursor into the templates is the key point.[79] For crystals with asymmetric structures, the subsequent annealing is capable of inducing self-assembly of nanoparticles preformed during the SCS procedure, especially for those in the molten salts, to achieve 1D nanostructures.[80–82] It still remains a challenge to directly obtain regular and uniform nanostructures by SCS. The exact mechanism for the formation of the unique nanostructure during SCS is still unclear because of the rapid and unknown combustion process. For asymmetric crystals with high purity, it is possible to achieve directly 1D structures because of the driving force for minimizing the total surface energy.[84] For 3D structures of flower-like particles, an appropriate combustion environment favoring the local sintering of the preformed nanoparticles is of importance.[88] Further work is needed to clarify the exact formation mechanism of the various morphologies. We believe a deep understanding on the nucleation and crystal growth procedure characteristic of SCS would help clarifying the formation of the specific nanostructure during SCS. *In situ* electron microscopic observation would be also helpful to understand the mechanism of morphology evolution during SCS.

4.2 Porous materials

Porous materials have promising applications in the various fields of gas sensors, catalysis, separation, energy storage and energy conversion.[89–91] Most methods for synthesis of porous materials demand the assistance of templates: hard templates (mesoporous silica, silica sphere, or polystyrene sphere) and soft templates (surfactants or block copolymers).[92,93] Because of the advantages of rapid and energy efficient, it is interesting to adopt SCS to synthesize porous materials, which is simple, template-free and low cost. Sometimes porous structures can be obtained as a result of the gas evolution during the combustion reaction; however, the pores are usually inhomogeneous and most of pore size is in tens of micrometers. It is of importance to obtain relatively homogeneous porous materials with pore sizes ranging from nanometers to several micrometers, which is favorable for gas or liquid diffusion and provides a relatively large surface area.

Phase and surface area of products in SCS are greatly affected by fuels and fuel/oxidizer ratio. Anatase TiO_2 with high specific surface area and disordered mesopores (Fig. 6a and b) was successfully synthesized through SCS by using many kinds of fuels, such as glycine,[94–97] urea,[98–101] hexamethylenetetramine,[95] and oxalyldihydrazide.[95] Zhang *et al.* obtained porous $Li_3V_2(PO_4)_3/C$ (as shown in Fig. 6c and d) with a surface area of 25.7 $m^2\ g^{-1}$ by annealing sucrose and combustion-driven amorphous precursor at 800 °C for 8 h in a N_2 atmosphere, and this material exhibited excellent electrochemical properties.[61] Mesoporous MgO with a surface area of 107 $m^2\ g^{-1}$ was obtained by SCS, which exhibited excellent fluoride removal capacity.[102] Mesoporous alumina with high surface area and narrow pore size distribution was also prepared by SCS in a fuel (urea)-lean condition. The surface area decreased with increasing amounts of urea.[103] However, the as-synthesized alumina was amorphous and the surface area greatly decreased upon the subsequent crystallization procedure.[103] It is still difficult to extend this procedure for synthesis of other porous oxides with relatively uniform pores because of the unknown and uncontrollable combustion process.[16]

Chen *et al.* is the first to introduce salts in SCS, which greatly increases the surface area of products in SCS.[104] The role of salts

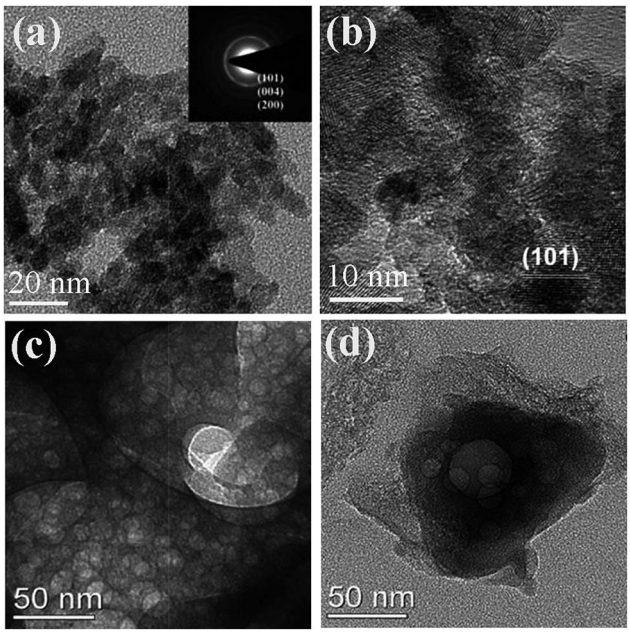

Fig. 6 (a) TEM image and (b) HRTEM image of TiO_2 with wormhole mesopores.[98] (c and d) TEM images of porous $Li_3V_2(PO_4)_3/C$.[61] (c and d) Adopted from ref. 61, Copyright 2012, with permission from Elsevier.

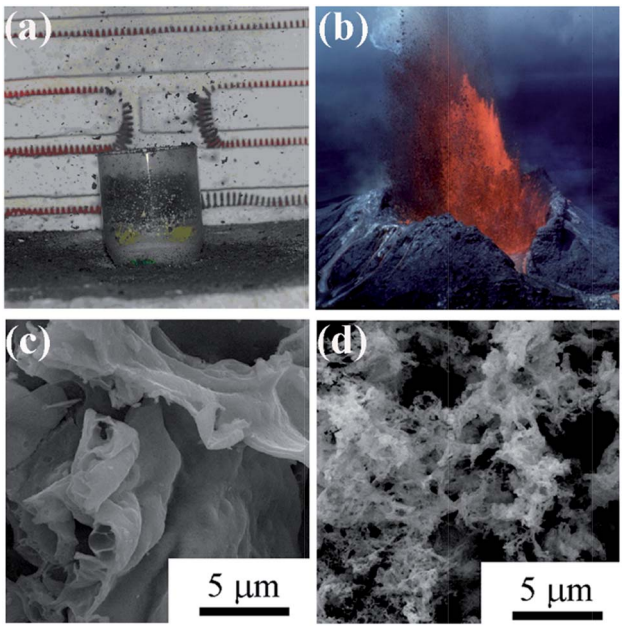

Fig. 7 Optical photographs of eruption combustion process (a) and volcanic eruption in nature (b). The optical photograph showing a natural volcanic eruption is from the Internet. SEM images of Ni/NiO powders derived with conventional combustion (c) and eruption combustion (d).[108] Adopted from ref. 108, Copyright 2011, with permission from American Chemical Society.

is believed to be two folds: decreasing the reaction temperature because the salt additives absorb reaction heat; salt precipitated *in situ* coats the newly formed nanoparticles, preventing them from sintering and agglomerating.[104–107] The salts are inexpensive and can be easily removed from the products by water washing. For the stoichiometric combustion reaction between nickel nitrate hexahydrate and citric acid, NaF is found to be more effective than NaCl for improving the surface area.[108] More interestingly, the additive of appropriate amounts of NaF alters the combustion mode, which results in the appearance of the so-called eruption combustion. In the eruption combustion process, lots of powders were lifted off and naturally fall down around the container, leaving highly fluffy products with a quite big volume, as shown in Fig. 7a. This phenomenon is very similar to a volcano eruption in nature (Fig. 7b). The eruption combustion in nickel nitrate–citric acid system resulted in smaller particles, improved dispersity, and remarkably increased specific surface area, as shown in Fig. 7c and d.[108] Moreover, it was shown that introduction of high surface area carriers in SCS also helps to obtain high surface area oxide-based supported catalysts.[109]

Fuel-rich conditions in SCS usually result in residual organics in the products. Carefully selecting fuels and adopting a high fuel/oxidizer ratio can obtain an organic-rich and amorphous precursor, which further decomposes to form porous metal oxide by the subsequent calcination because of gas evolutions. By using this method, homogeneously macroporous ZnO can be achieved, as shown in Fig. 8a and b.[110] The synthesis route can also be extended to the preparation of other porous oxides. For example, porous Co_3O_4 (Fig. 8c and d) can be also obtained by this method.[111] The decomposition

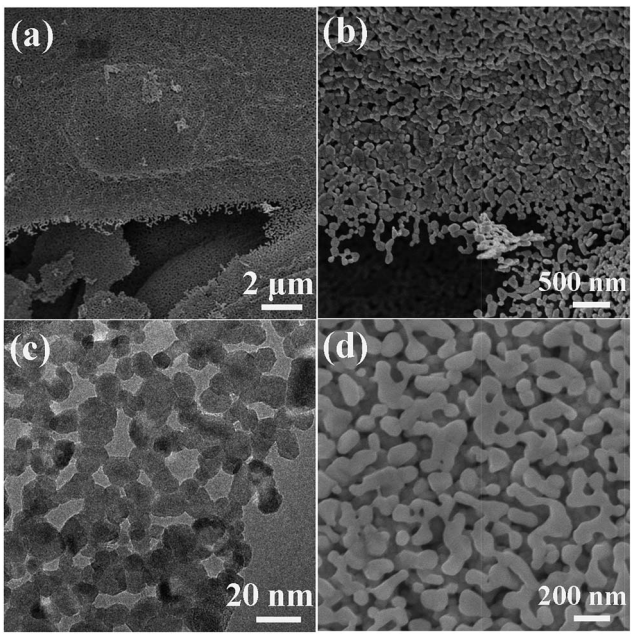

Fig. 8 (a and b) SEM images of porous ZnO network.[110] (c) TEM image of mesoporous Co_3O_4 calcined at 355 °C.[111] (d) SEM image of macroporous Co_3O_4 calcined at 550 °C.[111] (a and b) Adopted from ref. 110, Copyright 2012, with permission from AIP Publishing.

temperature of the Co-based precursor is much lower than that of the Zn-based precursor.[110,111] The low decomposition temperature of the Co-based precursor is beneficial for the

formation of the mesoporous Co_3O_4 network (Fig. 8c). Increasing the calcination temperature results in a larger particle size and larger pore size of the porous Co_3O_4, as shown in Fig. 8d, due to the enhanced grain growth.[111]

Hydrazine has a high energy N–N bond and lone electron pairs, which can coordinate with metal ions to form metal complexes.[15] Such metal hydrazine complexes can serve as precursors to be decomposed to corresponding oxide materials under low temperatures.[112–114] The energetic complexes usually decompose in an exothermal way along with combustion at low temperatures. Moreover, the raw materials for the complexes are water-soluble. Thus, the synthesis route starting from metal hydrazine complexes is very similar to the SCS procedure and can be classified as SCS. Recently we used metal nitrate, metal acetate, hydrazine hydrate, and glycine to synthesize homogeneous macroporous NiO/Ni[115] and porous ZnO.[116] The morphology of macroporous NiO/Ni can be changed by adjusting the complex composition. For example, macroporous NiO/Ni with three-dimensional (3D) and two-dimensional (2D) architectures can be achieved, as shown in Fig. 9a–d. The content of NiO in the macroporous NiO/Ni can be controlled by a subsequent calcination, with the macroporous structure preserved.[117] The obtained ZnO exhibits a coral-like macro-/mesoporous structure (Fig. 9e and f).[116] Interestingly, this kind of metal hydrazine complexes can transform to macro-/meso-/microporous nanofoam structures under focused electron beam irradiation during TEM operation. For example, porous ZnO nanofoams with ultrathin walls (Fig. 10a–c) are obtained *via* focused electron beam irradiation of the zinc hydrazine complex, whose preparation process is the same to that in the ref. 116 As shown in the HRTEM image (Fig. 10c), the measured lattice spacing of 0.25 nm and 0.26 nm represents the (101) and (002) atomic plane of wurtzite ZnO, respectively. The SAED pattern (Fig. 10d) further demonstrates that the product is polycrystalline wurtzite ZnO. This difference of morphology (comparing Fig. 10a–c with Fig. 9e and f) may be attributed to the different heating rates and atmospheric pressures. The much higher heating rate of the focused electron beam and lower atmospheric pressure during TEM operation result in the formation of porous nanofoams with ultrathin walls. This one-step route to porous structures is simple and rapid; however, hydrazine is toxic, and the reaction is relatively violent and hence careful operation and safety protection are required.

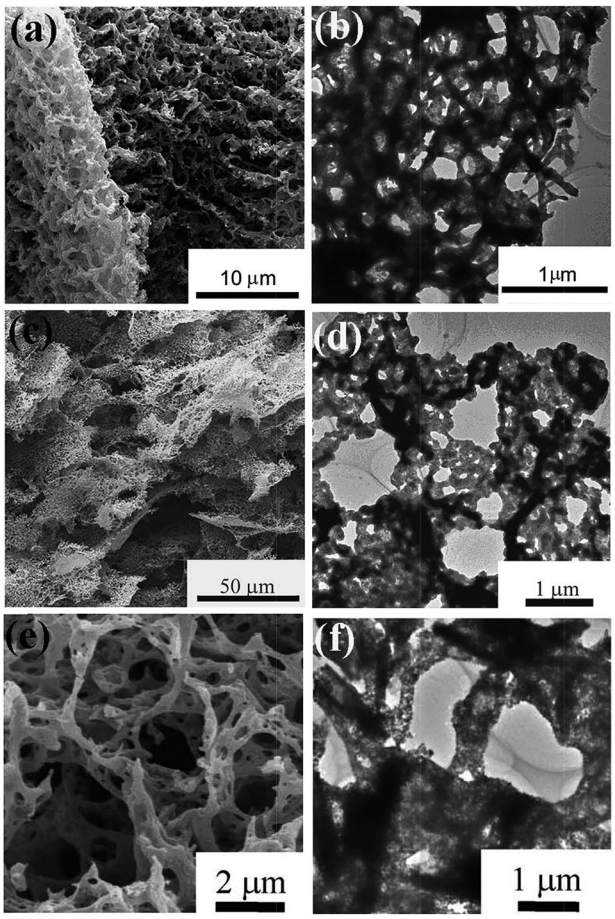

Fig. 9 SEM image (a) and TEM image (b) of 3D macroporous NiO/Ni. SEM image (c) and TEM mage (d) of 2D macroporous NiO/Ni.[115] SEM image (e) and TEM image (f) of 3D porous ZnO.[116] (a–d) Adopted from ref. 115, Copyright 2013, with permission from Elsevier.

4.3 Thin films

SCS is more commonly used to produce materials in form of powders. Many precursors employed in SCS have an uncanny resemblance to corresponding compounds utilized in sol–gel routes.[21] Thus, it is possible to obtain metal oxide thin films by SCS. Recently, Marks *et al.* adopt SCS as a new general route to fabricate diverse metal oxide thin films of In_2O_3, Zn–Sn–O, In–Zn–O, and ITO.[51] Taking the synthesis of ZnO films for example, 297.5 mg $Zn(NO_3)_2 \cdot 6H_2O$ and 100.1 mg urea were dissolved in 5 ml 2-methoxyethanol and aged for 72 h. Then, the

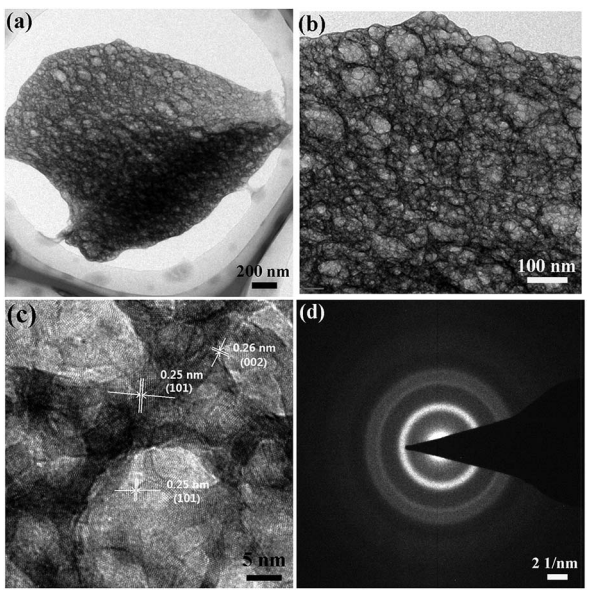

Fig. 10 TEM images (a, b), HRTEM image (c), and SAED pattern (d) of porous ZnO nanofoams derived from focused electron beam irradiation of the zinc hydrazine complex under TEM operation.

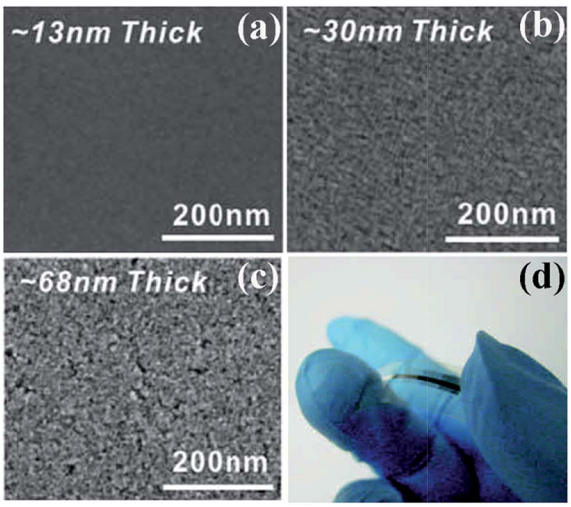

Fig. 11 (a–c) SEM images of In_2O_3 films on n++ Si with controlled thickness. (d) Optical image of a flexible combustion-processed In_2O_3 device.[51] Adopted from ref. 51, Copyright 2011, with permission from Macmillan Publishers Ltd.

films were fabricated by spin coating and annealed at the desired temperature (150–400 °C) for 30 min in air.[51] Fig. 11a–c shows the SEM images of SCS-derived In_2O_3 thin films with controlled thickness.[51] Thin films with a thickness of 30 nm or less exhibit smooth surfaces and negligible porosity; on the contrary, those with a thickness over 70 nm exhibit voids and evidence of porosity because of gas release during SCS. Growth of thicker and denser films thus demands multiple depositions.

The driving force of oxide lattice formations in SCS is from the internal chemical energy; therefore, the required temperature is just for reaction initiation rather than continuous energy input. These unique advantages endow SCS the ability to grow metal oxide films at temperatures as low as 200 °C.[51] It is thus convenient to achieve optically transparent transistors on flexible plastic substrates (Fig. 11d).[51,52] In a word, SCS enables the fabrication of low-cost and high-performance electronics at low temperatures.[51–55]

5. Conclusions and perspectives

Solution combustion synthesis has been adopted worldwide to synthesize numerous nanomaterials, especially simple and complex oxides, because of its simplicity, energy- and time-effectiveness, and low cost. The recent progress on controlled synthesis in SCS is described in detail in this review. It is a big challenge to obtain products with well defined phases and morphologies by SCS, which is partially attributed to the rapid and uncontrollable combustion procedure.

Besides the various metal oxides, it is now possible to synthesize metal sulfides, metals, and alloys, through careful selections of fuel and appropriate fuel/oxidant ratio. The metals or alloys are believed to result from the further reduction of the pre-formed corresponding metal oxides by the reducing atmosphere, which comes from either the excessive reducing fuel or the gas evolution during the combustion in fuel-rich conditions. The synthesis of other species, such as metal nitrides, metal carbides, and metal borides for a wider application still remains a challenge.

Oxides with regular morphologies of belts, triangles, tubes, wires, and rods can be synthesized by SCS, in the presence of certain templates, or through a self-assembly procedure. Utilizing the driving force for minimizing the total surface energy, SCS is capable of fabricating directly 1D structures when the target products are of asymmetric crystals. To achieve 3D structures of flower-like particles in one-step by SCS, an appropriate combustion environment should be maintained to favor the local sintering of the preformed nanoparticles to the resultants with specific morphologies.

More commonly, products in SCS are aggregates of nanoparticles, with relatively low specific surface area. The salt-assisted SCS favors the synthesis of oxides with small particles and thus high specific surface area. The additive of NaF in certain SCS system induced a novel eruption combustion mode, which further improves the dispersion and specific surface area of the produced oxides. Organic-rich precursor can be obtained by carefully selecting fuels and adopting a high fuel/oxidizer ratio, which further decomposes to form porous metal oxide by the subsequent calcination because of gas evolutions. Decomposition of metal hydrazine complexes is capable of producing oxides with high porosity. By adjusting the complex intensity, the architecture of the products can also be controlled. SCS is also developed to fabricate metal oxide thin films at low temperatures, enabling the fabrication of low-cost and high-performance electronics on flexible plastic substrates.

With the efforts of researchers worldwide, remarkable progresses have been made towards a more controllable SCS. However, the exact mechanism of SCS still remains unclear and it is a big challenge to achieve SCS products with well-defined phase structure and pre-designed morphology. Further work is needed to clarify the phase and microstructure evolution in the combustion process and to effectively control the combustion process.

Acknowledgements

This work is supported by the Natural Science Foundation of Zhejiang Province (Project no. LY13E020001). Dr Wen thanks a scholarship award for Excellent Doctoral Student granted by Ministry of Education, China for the financial support.

Notes and references

1 M. N. Rahaman, *Ceramic Processing and Sintering*, Marcel & Dekker, New York, 2nd edn, 1995.
2 *Chemical Processing of Ceramics*, ed. B. Lee and S. Komarneni, Taylor and Francis, New York, 2005.
3 A. S. Mukasyan, P. Epstein and P. Dinka, *Proc. Combust. Inst.*, 2007, **31**, 1789.
4 S. T. Aruna and A. S. Mukasyan, *Curr. Opin. Solid State Mater. Sci.*, 2008, **12**, 44.
5 H. Birol, C. R. Rambo, M. Guiotoku and D. Hotza, *RSC Adv.*, 2013, **3**, 2873.

6 K. C. Patil, S. T. Aruna and T. Mimani, *Curr. Opin. Solid State Mater. Sci.*, 2002, **6**, 507.
7 R. Rosa, P. Veronesi and C. Leonelli, *Chem. Eng. Process.*, 2013, **71**, 2.
8 J. J. Moore and H. J. Feng, *Prog. Mater. Sci.*, 1995, **39**, 243.
9 K. C. Patil, S. T. Aruna and S. Ekambaram, *Curr. Opin. Solid State Mater. Sci.*, 1997, **2**, 158.
10 Z. Du, H. Fu, H. Fu and Q. Xiao, *Mater. Lett.*, 2005, **59**, 1583.
11 F. Bernard and E. Gaffet, *Int. J. Self-Propag. High-Temp. Synth.*, 2001, **10**, 109.
12 L. Stobierski, Z. Wegrzyn, J. Lis and M. Buck, *Int. J. Self-Propag. High-Temp. Synth.*, 2001, **10**, 217.
13 I. P. Borovinskaya, T. I. Ignat'eva, V. I. Vershinnikov, G. G. Khurtina and N. V. Sachkova, *Inorg. Mater.*, 2003, **39**, 588.
14 J. J. Kingsley and K. C. Patil, *Mater. Lett.*, 1988, **6**, 427.
15 K. C. Patil, M. S. Hegde, R. Yanu and S. T. Atuna, *Chemistry of nanocrystalline oxide materials: combustion synthesis, properties and applications*, World Scientific, Singapore, 2008.
16 *Combustion synthesis: novel routes to novel materials*, ed. M. Lackner, Betham science publishers, 2010.
17 J. Lin, M. Yu, C. Lin and X. Liu, *J. Phys. Chem. C*, 2007, **111**, 5835.
18 S. R. Jain, K. C. Adiga and V. R. Pai Verneker, *Combust. Flame*, 1981, **40**, 71.
19 H. Q. Jiang, H. Endo, H. Natori, M. Nagai and K. Kobayashi, *J. Eur. Ceram. Soc.*, 2008, **28**, 2955.
20 W. Wen, J. M. Wu and Y. D. Wang, *Sens. Actuators, B*, 2013, **184**, 78.
21 K. Rajeshwar and N. R. de Tacconi, *Chem. Soc. Rev.*, 2009, **38**, 1984.
22 M. S. Hegde, G. Madras and K. C. Patil, *Acc. Chem. Res.*, 2009, **42**, 704.
23 K. Nagaveni, M. S. Hegde, N. Ravishankar, G. N. Subbanna and G. Madras, *Langmuir*, 2004, **20**, 2900.
24 K. R. Priolkar, P. Bera, P. R. Sarode, M. S. Hegde, S. Emura, R. Kumashiro and N. P. Lalla, *Chem. Mater.*, 2002, **14**, 2120.
25 X. Guo, D. Mao, G. Lu, S. Wang and G. Wu, *J. Catal.*, 2010, **271**, 178.
26 J. M. Wu and W. Wen, *Environ. Sci. Technol.*, 2010, **44**, 9123.
27 S. Pany, K. M. Parida and B. Naik, *RSC Adv.*, 2013, **3**, 4976.
28 W. Morales, M. Cason, O. Aina, N. R. de Tacconi and K. Rajeshwar, *J. Am. Chem. Soc.*, 2008, **130**, 6318.
29 S. L. Gonzalez-Cortes and F. E. Imbert, *Appl. Catal., A*, 2013, **452**, 117.
30 A. Zhao, W. Ying, H. Zhang, H. Ma and D. Fang, *Catal. Commun.*, 2012, **17**, 34.
31 S. Ekambarama, K. C. Patil and M. Maazac, *J. Alloys Compd.*, 2005, **393**, 81.
32 Z. Qiu, Y. Zhou, M. Lu, A. Zhang and Q. Ma, *Acta Mater.*, 2007, **55**, 2615.
33 V. Singh, S. Watanabe, T. K. G. Rao, K. Al-Shamery, M. Haase and Y. D. Jho, *J. Lumin.*, 2012, **132**, 2036.
34 Z. Qiu, Y. Zhou, M. Lü, A. Zhang and Q. Ma, *Solid State Sci.*, 2008, **10**, 629.
35 S. S. Yao, L. H. Xue and Y. W. Yan, *J. Alloys Compd.*, 2011, **509**, 1870.
36 S. S. Yao, L. H. Xue, Y. W. Yan and M. F. Yan, *J. Am. Ceram. Soc.*, 2011, **94**, 1477.
37 H. Mohebbi, T. Ebadzadeh and F. A. Hesari, *J. Power Sources*, 2008, **178**, 64.
38 M. A. Raza, I. Z. Rahman and S. Beloshapkin, *J. Alloys Compd.*, 2009, **485**, 593.
39 B. S. Prakash, V. K. W. Grips and S. T. Aruna, *J. Power Sources*, 2012, **214**, 358.
40 S. L. Chung and C. M. Wang, *J. Mater. Sci. Technol.*, 2012, **28**, 713.
41 S. A. Kelkar, P. A. Shaikh, P. Pachfule and S. B. Ogale, *Energy Environ. Sci.*, 2012, **5**, 5681.
42 K. Sivaranjani, S. Agarkar, S. B. Ogale and C. S. Gopinath, *J. Phys. Chem. C*, 2012, **116**, 2581.
43 P. Manikandan, M. V. Ananth, T. P. Kumar, M. Raju, P. Periasamy and K. Manimaran, *J. Power Sources*, 2011, **196**, 10148.
44 W. Wen, J. M. Wu and J. P. Tu, *J. Alloys Compd.*, 2012, **513**, 592.
45 G. T. K. Fey, Y. D. Cho and T. P. Kumar, *Mater. Chem. Phys.*, 2006, **99**, 451.
46 A. S. Prakash, P. Manikandan, K. Ramesha, M. Sathiya, J. M. Tarascon and A. K. Shukla, *Chem. Mater.*, 2010, **22**, 2857.
47 A. Huczko, M. Kurcz, P. Baranowski, M. Bystrzejewski, A. Bhattarai, S. Dyjak, R. Bhatta, B. Pokhrel and B. P. Kafle, *Phys. Status Solidi B*, 2013, **250**, 2702.
48 K. Suresh, N. R. S. Kumar and K. C. Patil, *Adv. Mater.*, 1991, **3**, 148.
49 K. Laishram, R. Mann and N. Malhan, *Ceram. Int.*, 2011, **37**, 3743.
50 M. B. Kakadea, S. Ramanathana and P. V. Ravindran, *J. Alloys Compd.*, 2003, **350**, 123.
51 M. G. Kim, M. G. Kanatzidis, A. Facchetti and T. J. Marks, *Nat. Mater.*, 2011, **10**, 382.
52 Y. S. Rim, H. S. Lim and H. J. Kim, *ACS Appl. Mater. Interfaces*, 2013, **5**, 3565.
53 J. W. Hennek, M. G. Kim, M. G. Kanatzidis, A. Facchetti and T. J. Marks, *J. Am. Chem. Soc.*, 2012, **134**, 9593.
54 M. G. Kim, J. W. Hennek, H. S. Kim, M. G. Kanatzidis, A. Facchetti and T. J. Marks, *J. Am. Chem. Soc.*, 2012, **134**, 11583.
55 D. Sanchez-Rodriguez, J. Farjas, P. Roura, S. Ricart, N. Mestres, X. Obradors and T. Puig, *J. Phys. Chem. C*, 2013, **117**, 20133.
56 A. Cüneyt Tas, *J. Eur. Ceram. Soc.*, 2000, **20**, 2389.
57 S. Gallini, J. R. Jurado and M. T. Colomer, *Chem. Mater.*, 2005, **17**, 4154.
58 M. T. Colomer, S. Gallini and J. R. Jurado, *J. Eur. Ceram. Soc.*, 2007, **27**, 4237.
59 I. M. Nagpure, K. N. Shinde, V. Kumar, O. M. Ntwaeaborwa, S. J. Dhoble and H. C. Swart, *J. Alloys Compd.*, 2010, **492**, 384.
60 B. Zhao, X. Yu, R. Cai, R. Ran, H. Wang and Z. Shao, *J. Mater. Chem.*, 2012, **22**, 2900.

61 L. Zhang, H. Xiang, Z. Li and H. Wang, *J. Power Sources*, 2012, **203**, 121.
62 M. Pardha Saradhi and U. V. Varadaraju, *Chem. Mater.*, 2006, **18**, 5267.
63 M. Dahbi, S. Urbonaite and T. Gustafsson, *J. Power Sources*, 2012, **205**, 456.
64 D. Wang, B. A. Doull, L. C. Oliveira and E. G. Yukihara, *RSC Adv.*, 2013, **3**, 26127.
65 R. K. Tukhtaev, V. V. Boldyrev, A. I. Gavrilov, S. V. Larionov, L. I. Myachina and Z. A. Savel'eva, *Inorg. Mater.*, 2002, **38**, 985.
66 S. Arora and S. S. Manoharan, *J. Phys. Chem. Solids*, 2007, **68**, 1897.
67 R. Amutha, M. Muruganandham, G. J. Lee and J. J. Wu, *J. Nanosci. Nanotechnol.*, 2011, **11**, 7940.
68 G. R. Rao, B. G. Mishra and H. R. Sahu, *Mater. Lett.*, 2004, **58**, 3523.
69 C. H. Jung, S. Jalota and S. B. Bhaduri, *Mater. Lett.*, 2005, **59**, 2426.
70 P. Erri, J. Nader and A. Varma, *Adv. Mater.*, 2008, **20**, 1243.
71 Y. Jiang, S. Yang, Z. Hua and H. Huang, *Angew. Chem., Int. Ed.*, 2009, **48**, 8529.
72 A. Kumar, E. E. Wolf and A. S. Mukasyan, *AIChE J.*, 2010, **57**, 2207.
73 A. Kumar, E. E. Wolf and A. S. Mukasyan, *AIChE J.*, 2011, **12**, 3473.
74 K. V. Manukyan, A. Cross, S. Roslyakov, S. Rouvimov, A. S. Rogachev, E. E. Wolf and A. S. Mukasyan, *J. Phys. Chem. C*, 2013, **117**, 24417.
75 Z. Hua, Y. Deng, K. Li and S. Yang, *Nanoscale Res. Lett.*, 2012, **7**, 129.
76 Z. H. Hua, Z. W. Cao, Y. Deng, Y. W. Liang and S. G. Yang, *Mater. Chem. Phys.*, 2011, **126**, 542.
77 P. Gómez-Romero, J. Frailec and B. Ballesteros, *RSC Adv.*, 2013, **3**, 2351.
78 A. Kumara, J. T. Miller, A. S. Mukasyan and E. E. Wolf, *Appl. Catal., A*, 2013, **467**, 593.
79 Y. Yuan, C. S. Liu, Y. Zhang and X. Q. Shan, *Mater. Chem. Phys.*, 2008, **112**, 275.
80 J. Ding, S. Sun, J. Bao, Z. Luo and C. Gao, *Catal. Lett.*, 2009, **130**, 147.
81 P. A. Deshpande and G. Madras, *AIChE J.*, 2011, **57**, 2215.
82 W. Chen, M. Liu, Y. Lin, Y. Liu, L. Yu, T. Li and J. Hong, *Ceram. Int.*, 2013, **39**, 7545.
83 S. Jalota, A. C. Tas and S. B. Bhaduri, *J. Mater. Res.*, 2004, **19**, 1876.
84 X. Y. Tao, X. N. Wang and X. D. Li, *Nano Lett.*, 2007, **7**, 3172.
85 B. C. Cheng, Z. D. Zhang, H. J. Liu, Z. H. Han, Y. H. Xiao and S. J. Lei, *J. Mater. Chem.*, 2010, **20**, 7821.
86 B. C. Cheng, Z. D. Zhang, Z. H. Han, Y. H. Xiao and S. J. Lei, *CrystEngComm*, 2011, **13**, 3545.
87 M. Mapa and C. S. Gopinath, *Chem. Mater.*, 2009, **21**, 351.
88 M. Umadevi and A. J. Christy, *Spectrochim. Acta, Part A*, 2013, **109**, 133.
89 V. Valtchev and L. Tosheva, *Chem. Rev.*, 2013, **113**, 6734.
90 N. D. Petkovich and A. Stein, *Chem. Soc. Rev.*, 2013, **42**, 3721.
91 A. Stein, B. E. Wilson and S. G. Rudisill, *Chem. Soc. Rev.*, 2013, **42**, 2763.
92 X. Chen, J. Ye, S. Ouyang, T. Kako, Z. Li and Z. Zou, *ACS Nano*, 2011, **5**, 4310.
93 J. M. Wu, M. Antonietti, S. Gross, M. Bauer and B. M. Smarsly, *ChemPhysChem*, 2008, **9**, 748.
94 G. Sivalingam, K. Nagaveni, M. S. Hegde and G. Madras, *Appl. Catal., B*, 2003, **45**, 23.
95 K. Nagaveni, M. S. Hegde, N. Ravishankar, G. N. Subbanna and G. Madras, *Langmuir*, 2004, **20**, 2900.
96 K. Nagaveni, M. S. Hegde and G. Madras, *J. Phys. Chem. B*, 2004, **108**, 20204.
97 A. D. Mani, V. Laporte, P. Ghosal and C. Subrahmanyam, *Mater. Res. Bull.*, 2012, **47**, 2415.
98 K. Sivaranjani and C. S. Gopinath, *J. Mater. Chem.*, 2011, **21**, 2639.
99 K. Sivaranjani, S. Agarkar, S. B. Ogale and C. S. Gopinath, *J. Phys. Chem. C*, 2012, **116**, 2581.
100 S. S. Negi, K. Sivaranjani, A. P. Singh and C. S. Gopinath, *Appl. Catal., A*, 2013, **452**, 132.
101 S. Pany, K. M. Parida and B. Naik, *RSC Adv.*, 2013, **3**, 4976.
102 B. Nagappa and G. T. Chandrappa, *Microporous Mesoporous Mater.*, 2007, **106**, 212.
103 M. Pavese and S. Biamino, *J. Porous Mater.*, 2009, **16**, 59.
104 W. Chen, F. Li, J. Yu and L. Liu, *Mater. Sci. Eng., B*, 2006, **133**, 151.
105 W. Chen, J. Hong and Y. Li, *J. Alloys Compd.*, 2009, **484**, 846.
106 X. Zhang, W. Jiang, D. Song, H. Sun, Z. Sun and F. Li, *J. Alloys Compd.*, 2009, **475**, L34.
107 Y. Tong, S. Zhao, X. Wang and L. Lu, *J. Alloys Compd.*, 2009, **479**, 764.
108 W. Wen and J. M. Wu, *ACS Appl. Mater. Interfaces*, 2011, **3**, 4112.
109 P. Dinka and A. S. Mukasyan, *J. Phys. Chem. B*, 2005, **109**, 21627.
110 W. Wen, J. M. Wu and Y. D. Wang, *Appl. Phys. Lett.*, 2012, **100**, 262111.
111 W. Wen, J. M. Wu and M. H. Cao, *Nanoscale*, 2014, **6**, 12476.
112 K. C. Patil, *Proc.–Indian Acad. Sci., Chem. Sci.*, 1986, **96**, 459.
113 T. T. Srinivasan, P. Ravindranathan, L. E. Cross, R. Roy, R. E. Newnham, S. G. Sankar and K. C. Patil, *J. Appl. Phys.*, 1988, **63**, 3789.
114 J. W. Park, E. H. Chae, S. H. Kim, J. H. Lee, J. W. Kim, S. M. Yoon and J. Y. Choi, *Mater. Chem. Phys.*, 2006, **97**, 371.
115 W. Wen, J. M. Wu and M. H. Cao, *Nano Energy*, 2013, **2**, 1383.
116 W. Wen, J. M. Wu and Y. D. Wang, *RSC Adv.*, 2013, **3**, 12052.
117 W. Wen, J. M. Wu and M. H. Cao, *J. Mater. Chem. A*, 2013, **1**, 3881.

